Antibacterial -Glucan/Zinc Oxide Nanocomposite Films for Wound Healing

BioNanoScience (2023) 13:426–435
https://doi.org/10.1007/s12668-023-01079-0

Antibacterial β-Glucan/Zinc Oxide Nanocomposite Films for Wound Healing

Paolo Pino[1] · Giorgia Pellegrino[1] · Silvia Ronchetti[1] · Chiara Mollea[1] · Francesca Bosco[1] · Barbara Onida[1]

Accepted: 8 March 2023 / Published online: 17 March 2023

Abstract
Advanced antimicrobial biomaterials for wound healing applications are an active field of research for their potential in addressing severe and infected wounds and overcoming the threat of antimicrobial resistance. Beta-glucans have been used in the preparation of these materials for their bioactive properties, but very little progress has been made so far in producing biomedical devices entirely made of beta-glucans and in their integration with effective antimicrobial agents. In this work, a simple and eco-friendly method is used to produce flexible beta-glucan/nanostructured zinc oxide films, using glucans derived from the yeast *Saccharomyces cerevisiae*. The properties of the films are characterized through scanning electron microscopy, energy-dispersive X-ray spectroscopy, X-ray photoelectron spectroscopy, X-ray diffraction, infrared and UV–visible spectroscopy, thermogravimetric analysis, differential scanning calorimetry, and water absorption tests. Finally, the antibacterial properties of the nanostructured zinc oxide and of the composite films are assessed against *Staphylococcus epidermidis* and *Escherichia coli*, showing a marked effectiveness against the former. Overall, this study demonstrates how a novel bionanocomposite can be obtained towards the development of advanced wound healing devices.

Keywords Beta-glucans · Nanostructured zinc oxide · Antibacterial bionanocomposites · Wound healing

1 Introduction

Wounds are a major burden for healthcare, quality of life, and the economy. The presence of acute or chronic wounds determines a substantial decrease in the patient's quality of life and a corresponding increase in associated wound care costs. The economic and healthcare burdens of wounds are expected to grow due to the aging population in most countries and to the early development of illnesses that are typically connected to wound insurgence, such as diabetes and obesity [1].

An additional negative spill-over of this global issue is the indirect cost generated by the decrease in productivity experienced by tens of millions of wounded individuals.

On top of all that, wounds are frequently subjected to infections caused by rapid bacterial colonization of the wound area. Infection can interfere with the normal healing process and frequently gives rise to more serious implications. For instance, surgical site infections contribute to 75% of post-surgery deceases [2].

As regard direct and indirect costs related to wound dressing management, the USA alone annually spend more than 25 billion dollars [3]. At the same time, in the main European countries, the mean annual costs due a patient hospitalized for wound problems are estimated to be about 10.000 euros [4]. In this aim, the worldwide expenditure is expected to reach 80 billion dollars by the year 2024 [4, 5].

A consequence of this trend is a corresponding increase in the global demand for advanced wound care products. The related market was valued $6.5 billion in 2020 and is expected to grow steadily in the forthcoming years [6].

Thousands of wound dressings are already commercially available, covering the large span of needs and requirements associated to different types of wounds. These solutions have limitations, such as the use of crosslinking agents, toxic decomposition by-products, painful removal, poor exudate absorption ability, or the use of petroleum-based raw materials. Researchers are developing new, advanced strategies to address these gaps, such as biopolymers-based, medicated, and composite dressings made of natural biomacromolecules

✉ Francesca Bosco
francesca.bosco@polito.it

[1] Department of Applied Science and Technology, Politecnico Di Torino, Corso Duca Degli Abruzzi 24, 10129 Torino, Italy

like chitosan, collagen, and cellulose [7, 8]. These combine the high biocompatibility and environmental sustainability of biopolymers with the beneficial effects of incorporated medications, such as antibiotics. Within this domain, beta-glucans (BG) are gaining increasing attention in the fabrication of wound dressings thanks to their immunostimulatory properties. In fact, the innate immune receptor Dectine-1 recognizes beta-glucans as pathogen-associated molecular patterns (PAMPs), thus triggering an immune response [9] and proliferation of keratinocytes in humans [10], as well as other skin health promotion effects [11]. BG have been used as additives for the fabrication of nanofibrous [12] and sprayable dressings [13] and blended with gelatin [14], poly(vinyl alcohol) [15], starch [16], and pullulan [17]. Different types of BG gels for wound healing have also been reported in the literature [18, 19].

However, very little research exists on the fabrication of BG films, which would constitute another important contribution to the development of wound dressings based on natural biomacromolecules by expanding the range of possible applications thanks to their particular properties. As a next step in this direction, novel films with biomedical properties introduced by the addition of therapeutic and antimicrobial agents would further improve their effectiveness and would substantially advance the quality of healthcare and patient lifestyle.

The most common microbial species isolated from infected wounds are gram-negative bacteria (57.9%), with a prevalence of *Pseudomonas aeruginosa* (40.2%), *Escherichia coli* (20.7%), *Proteus mirabilis* (11.2%), and *Acinetobacter baumannii/haemolyticus* (9.5%). On the other side, gram-positive bacteria represent the 36.6%, with *Staphylococcus aureus* as the predominant specie (79.4%); this last appears to be the most frequent colonizer in the initial phase of infections, and it is well-known for its involvement in antimicrobial resistance (AMR) [20]. AMR is one of the biggest public health challenges of our time, claiming at least 700,000 lives per year worldwide. Within the context, nanostructured zinc oxide (nZnO) is known for its marked antimicrobial, anticancer, and anti-inflammatory properties, as well as for its biocompatibility and ability to stimulate keratinocytes proliferation [21, 22]. ZnO NPs exhibit antimicrobial property against both gram-positive and gram-negative bacteria and also against fungi. The antimicrobial activity of ZnO NPs may be due to the release of Zn^{2+} ions, reactive oxygen species (ROS) production, and physical interactions with the cellular membrane [23].

Given its multiple mechanisms of antimicrobial action, different than those expressed by traditional drugs and antibiotics, nZnO is also a good candidate to contrast drug-resistant strains. All these properties make nZnO a very well-suited material for wound healing and skin tissue engineering. In a recent review on wound-healing therapy, nanocomposites based on ZnO NPs entrapped in chitosan hydrogel, collagen dressing, or cellulose sheets were described; in all the cases, both antibacterial and tissue regeneration activity were reported [24]. Moreover, ZnO NPs incorporated in hydrogel-based wound dressings allow to increase the overall contact time with the wound and to promote keratinocyte migration, improving re-epithelialization [25].

Despite this, only a study by Razzaq et al. has demonstrated the antimicrobial properties of ZnO containing BG films obtained from barley [26] so far.

However, the ZnO used in this study was 500 nm in size. It is known that nanostructured zinc oxide (with sizes typically ranging from 1 to 100 nm) possesses greater antimicrobial activity thanks to its reduced size [27]. Furthermore, there is a large body of scientific evidence suggesting that β-glucans from *Saccharomyces cerevisiae* promote wound healing and skin repair processes by stimulating fibroblast proliferation and growth factor expression [28], which would be highly desirable properties for innovative wound dressings. In fact, the biological activity of β-glucans is dependent on their source and structural conformation [29]. However, β-glucans from *S. cerevisiae* are not water soluble, contrary to cereal-derived ones, thus making the fabrication of medical devices more difficult. Overcoming this limitation would be a significant progress towards the development of multifunctional, advanced wound dressings.

In this study, a simple fabrication route for the obtainment of flexible composite beta-glucan/nanostructured zinc oxide (BGZ) films using commercial *S. cerevisiae* β-glucans is presented. The nanocomposites are then characterized and tested against two bacterial strains, namely, gram-positive *Staphylococcus epidermidis* and gram-negative *Escherichia coli*, to assess antibacterial efficacy.

2 Materials and Methods

Zinc acetate di-hydrate (≥ 98%), potassium hydroxide (≥ 85%), absolute ethanol, and glycerol (≥ 99%) were obtained from Sigma-Aldrich (St. Louis, MO, USA) and used as received. Beta-glucan powders (70%) were purchased from ACEF S.p.A. (Fiorenzuola d'Arda, Piacenza, Italy). Mueller Hinton Broth CM0405 (MHB) and Mueller Hinton Agar CM0337 (MHA) were supplied by OXOID Ltd (Basingstoke, United Kingdom).

2.1 Synthesis of nZnO

Nanostructured zinc oxide is obtained through a wet chemical precipitation technique previously adopted in another study [30]. Briefly, 14.75 g of zinc acetate dihydrate and 7.4 g of potassium hydroxide are dissolved in 60 and 32 mL

of ethanol, respectively. The two solutions are then mixed and kept at 70 °C for 72 h under constant agitation and solvent refluxing. The white precipitate is then collected by centrifugation, washed with ethanol, and dried in an oven for 24 h at 60 °C.

2.2 Characterization of nZnO

The crystal structure of nZnO powder was characterised through X-ray diffraction (XRD) using a PANalytical X'Pert Diffractometer (Cu K radiation, Almelo, The Netherlands). The X-ray diffraction pattern shows a wurtzite-type crystal structure, as previously reported [30].

The morphology of the nanoparticles was investigated by means of field emission scanning electron microscopy (FESEM) carried out with a ZEISS Merlin instrument (Oxford Instruments, Abingdon-on-Thames, UK). The ImageJ software (open source, https://imagej.net/, accessed 26 August 2021) was then used to measure particle size distribution. Zinc oxide nanoparticles are characterized by a spherical morphology and a size of 32 nm, as previously reported [30]. Specific surface area was determined through nitrogen physisorption measurements, performed using a ASAP2020 Plus Micromeritics apparatus (Norcross, GA, USA). Samples were degassed at 70 °C for 2 h. The specific surface area (SSA) was determined based on the Brunauer–Emmet–Teller (BET) model in the relative pressure p/p^0 range of 0.01–0.1. The SSA resulted to be about 50 m^2/g.

2.3 Preparation of BG Films

Beta-glucan films have been prepared following a procedure previously described by Sagnelli and co-workers [16] with some modifications. A 2% (w/v) BG suspension in distilled water was prepared and heated at 95 °C for 40 min to facilitate beta-glucan dispersion. After thermal treatment, glycerol was added in an amount equal to 25% of the dry weight of BG powder. After stirring, the suspension was poured onto 9-cm diameter polypropylene Petri dishes, maintaining a volume-to-surface ratio equal to 0.200 m. The dishes were placed in an oven for 3 h at 60 °C for solvent evaporation and film formation, and the films were subsequently peeled off and used for further characterization and testing.

2.4 Preparation of BGZ Films

For the preparation of composite films, a suspension of nZnO in water was prepared and sonicated in an ultrasonic bath for 1 h. The suspension was then added to the film forming BG suspension, subsequent to the heat treatment and glycerol addition. The mixture was then casted on Petri dishes, dried, and composite films were eventually obtained. Three different types of composite films were prepared, based on the nZnO content introduced in the matrix, namely, 2%, 4%, and 6% of the dry BG mass. The samples were therefore labeled BGZ-2, BGZ-4, and BGZ-6, respectively.

2.5 Characterization of Films

BG and BGZ films were characterised by means of X-ray diffraction using a PANalytical X'Pert Diffractometer (Cu K radiation, Almelo, The Netherlands) and scanning electron microscopy via a ZEISS Supra 40 field emission scanning electron microscope (ZEISS, Oberkochen, Germany). Cross sections of the films were imaged after immersing and subsequently fracturing samples in liquid nitrogen. Before the analysis, samples were coated with a 8-nm thick Pt layer. Energy-dispersive X-ray spectroscopy (EDS) was carried with an Oxford EDS Microanalysis (liquid N_2 cooled Si(Li) detector) instrument (Oxford Instruments, Abingdon, UK). X-ray photoelectron spectroscopy (XPS) was performed with a Physical Electronics VersaProbe apparatus (Physical Electronics, Lake Drive, MN, USA), using Al radiation ($h\upsilon = 1248$ eV). The C1s component at 284.8 eV was taken as a reference for the energy scale.

Spectroscopic characterization was carried out by means of UV–Vis spectroscopy, using a Lambda 465 UV/Vis spectrophotometer (PerkinElmer, Waltham, MA, USA), as well as attenuated total reflectance Fourier-transform infrared spectroscopy (ATR-FTIR), using a Nicolet iS50 FTIR Spectrometer equipped with Smart iTX optics and diamond crystal (Thermo Fischer Scientific, Waltham, MA, USA). Thermal properties were investigated through differential scanning calorimetry (DSC) and thermogravimetric analysis (TGA) using a Linseis STA PT 1600 apparatus (Linseis Messgeraete GmbH, Selb, Germany) in an inert argon atmosphere in the 25–800 °C temperature range, with a 10 °C/min heating rate. Glass transition temperature T_g was determined through the first derivative method.

2.6 Swelling Tests

For swelling tests, BG and BGZ films have been cut into 20-mm diameter discs, weighted, and dried in an oven at 60 °C until stabilization of the dry mass, m_d. Discs were then immersed in 20 mL of distilled water at different pH values, namely, 3, 5, 7, 9, and 11. Films were extracted from the liquid at 30 min time intervals, freed from excess water, and weighted until stabilization of the wet mass, m_w. Finally, the swelling ratio, SR, was determined as:

$$SR = \frac{m_w - m_d}{m_d} \bullet 100$$

Each experiment was repeated in triplicate.

2.7 Antibacterial Activity of nZnO

The minimum inhibitory concentration (MIC) and the minimum bactericidal concentration (MBC) of nZnO were determined applying the EUCAST broth microdilution method with some modifications [31]. The tested bacteria were the gram-positive *Staphylococcus epidermidis*, LMG 10,474, and the gram-negative *Escherichia coli*, LMG 08,063. A standardised inoculum, corresponding to 5×10^5 CFU/mL, was obtained by dispersing three colonies, taken from an overnight culture grown on MHA at 37 °C, into 5 mL of sterile 0.85% w/v NaCl solution and opportunely diluting the suspension with MHB. The 96-well plates were filled with 10 µL of inoculum, 50 µL of MHB, and 50 µL of nZnO suspensions with oxide concentrations ranging from 30 to 20,000 µg/mL. In the biotic controls, the nZnO suspensions were substituted with 50 µl of MHB, while in the abiotic ones the inoculum was substituted with 10 µl of MHB.

MIC was established as the lowest nZnO concentration capable of completely inhibit the growth of the bacteria as detected by the unaided eye. MBC was determined subculturing, on MHA, 10 µL of the broth dilutions that inhibited bacterial growth (those at or above the MIC); the MBC was the lowest broth dilution of nZnO that prevented the bacterial growth on MHA after 24 h of incubation at 37 °C.

2.8 Antimicrobial Activity of Composite Films

The antimicrobial activity of BG and BGZ films was assessed applying the EUCAST disk diffusion method with some modifications [32]; also in this case, the tested microorganisms have been *S. epidermidis* LMG 10,474 and *E. coli* LMG 08,063.

A standardised inoculum was prepared using the direct colony suspension method obtaining a bacterial suspension, in 0.85% NaCl, corresponding to $1–2\times10^8$ CFU/mL. A total of 100 µL of the inoculum were spread on MHA plates (Ø 90 mm) and 18 mm diameter BG, BGZ-2, BGZ-4, and BGZ-6 discs were gently deposited on the agar surface. Filter paper discs were used as negative controls. Plates were then incubated at 37 °C for 24 h. At the end of the incubation period, the antibacterial activity was measured as the average distance between the limit of the film disc and the inhibition halo edge, as judged by the naked eyed, for two perpendicular disc diameters. Each experiment was done in triplicate.

3 Results and Discussion

3.1 Characterization of Films

The film formation procedure described above led to the formation of flexible films. FESEM images in Fig. 1 showed that films have a compact microstructure. BG films (Fig. 1, A1) have a continuous and irregular surface, and EDS analysis reveals the presence of carbon and oxygen, as expected (Fig. 1, A2). The addition of ZnO (Fig. 1, B1) seems to cause an increase in surface roughness. This is caused by the presence of ZnO nanoparticles and their aggregates, as revealed by the EDS analysis. Figure 1, B2.1 shows that nZnO is homogeneously distributed in the composite film. Moreover, Fig. 1, B2.2 shows a several-micron-large nZnO aggregate, as confirmed by the overlap between the oxygen and zinc elemental maps and by the corresponding lack of carbon presence in the same area. In order to verify that nZnO was also dispersed across the thickness of the film, cross section images and elemental maps were taken. The inner part of the film is featured by micrometric pores, as shown in Fig. 1, A3 for the BG matrix. When nZnO is dispersed, porosity is preserved, but the nanoparticles and their aggregates become visible in the cross section as well (Fig. 1, B3). As a further confirmation, zinc was detected across the lateral section by EDS, as shown in Fig. 1, B4.

Figure 2 shows the results of the XPS analysis. A survey carried out on the four samples confirmed that nZnO was successfully included in the composite samples (Fig. 2A). The binding energy of Zn2p3 between 1022.13 and 1022.25 eV (Fig. 2B) in the four samples is between that reported for zinc hydroxide and zinc carbonate [33]. This suggests that a layer of hydroxylated and carbonate species was formed on the surface of the nanoparticles, as previously reported for a similar nanostructured zinc oxide [34]. As further confirmation, a FTIR analysis of the nZnO was carried using a Bruker Equinox 55 spectrometer (Bruker, Billerica, MA, USA), on a self-supported nZO pellet diluted in KBr after outgassing the powder at room temperature for 1 h at 0.1 Pa. The FTIR spectrum (Figure S1) confirmed the presence of surface hydroxyl groups (broad band at 3390 cm^{-1} ascribed to interacting hydroxyl species) and of surface carbonate species (bands in the 1700–1300 cm^{-1} range) [35].

The bulk phase of the nanoparticles is however not affected, as revealed by the XRD spectrum shown in Fig. 3, where the XRD patterns of the nZnO powder and of the four films are reported. The pattern observed for nZnO (grey line) is typical of the hexagonal wurtzite-like phase, as expected [30].

The patterns of the films reveal an amorphous structure in all cases, with a broad reflection at approximately $2\theta = 20$ which is consistent with literature data [16, 17]. The amorphous pattern is indicative of the formation of a dense molecular network, as proposed by Chang et al. [17], in agreement with the evidence obtained by FESEM analysis. Diffraction peaks attributable to nZnO are observed in the BGZ-4 and in the BGZ-6 samples thanks to the higher amount of oxidic phase. The presence of nZnO does not appear to affect the amorphous nature of the beta-glucan matrix.

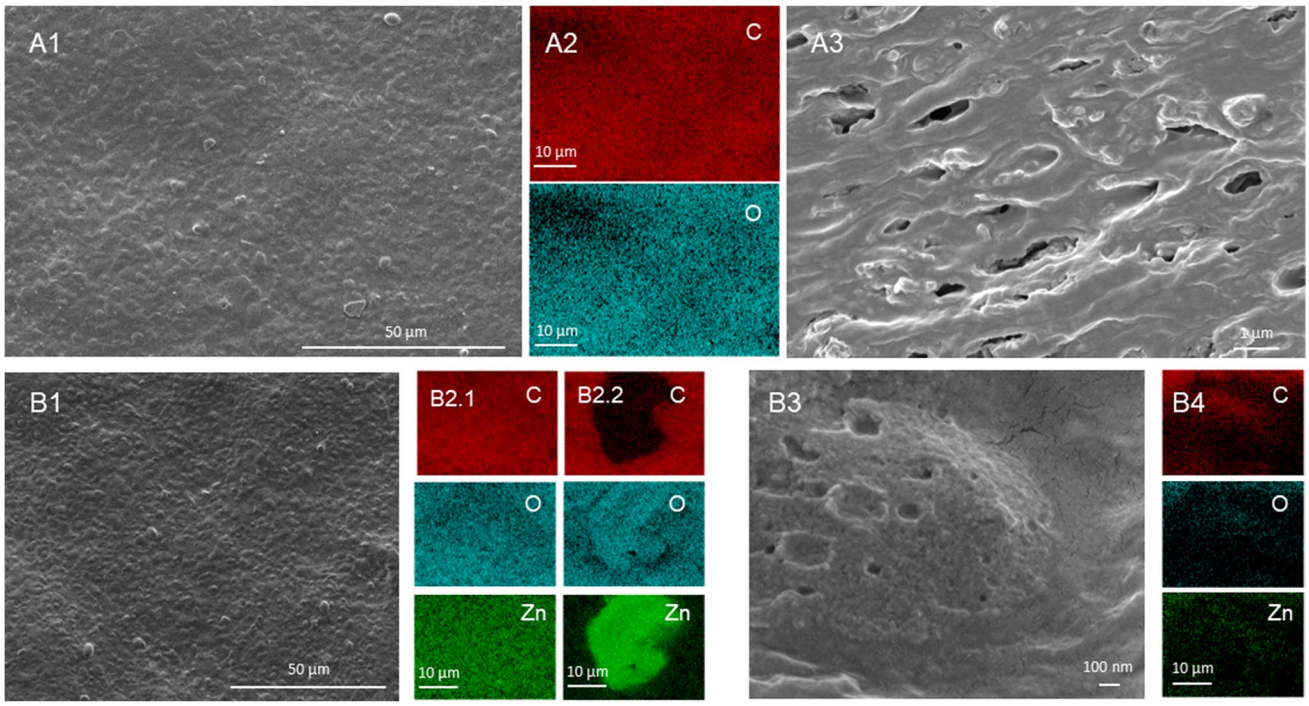

Fig. 1 (**A1**) FESEM image of BG film surface; (**A2**) EDS carbon and oxygen distribution map of BG film surface; (**A3**) FESEM image of BG film cross section; (**B1**) FESEM image of BGZ-6 film surface; (**B2**) elemental maps of C, O, and Zn of the BGZ-6 film surface in a generic point of the sample (B2.1) and in correspondence of a nZnO aggregate (B2.2); (**B3**) close-up FESEM image of a nZnO aggregate in the BGZ-6 film cross section; and (**B4**) elemental maps of C, O, and Zn in the BGZ-6 film cross section

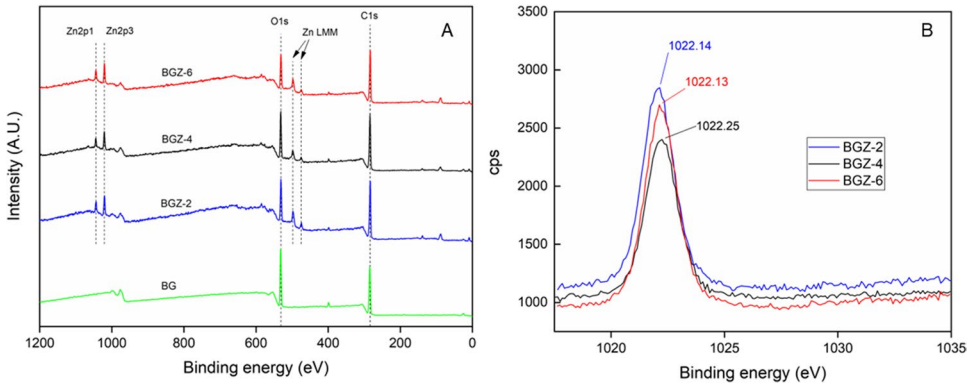

Fig. 2 **A** XPS survey of the samples and **B** high-resolution XPS peaks of Zn2p3

The ATR-FTIR spectra of BG and BGZ films are shown in Fig. 4. The broad band at about 3290 cm^{-1} is due to -OH groups, whereas the two peaks at about 2920 cm^{-1} and 2860 cm^{-1} are attributed to the asymmetric and symmetric $-CH_2$ group stretching, respectively [35]. Two weak bands are at 1635 cm^{-1} and 1560 cm^{-1}, which may be ascribed to amide groups, which might be retained in the BG extraction process [36]. The very strong bands in the 1010–1050 cm^{-1} range are typically found in glucans [36, 37]. The presence of nZnO does not result in any changes of the BGZ spectra with respect to the bare BG film.

Results of thermogravimetric analyses are shown in Fig. 5 (left side). After an initial weight loss due to evaporation of water, a second mass reduction onsets at approximately 200 °C due to the thermal decomposition of β-glucans [26], followed by a steeper mass loss step starting in the proximity of 300 °C, assigned to glycerol removal in addition to polysaccharide decomposition. The corresponding mass loss results to be around 25%, which is in agreement with the glycerol content from the preparation procedure.

In the last portion of the curves, between 400 °C and 800 °C, a further mass loss, of about 10%, is observed for BG and BGZ-2, whereas only a minor mass loss is observed for BGZ-4 and BGZ-6 in the same temperature range. The higher amount of residual mass in BGZ-4 and BGZ-6 can be attributed to the effect of ZnO nanoparticles, which absorb

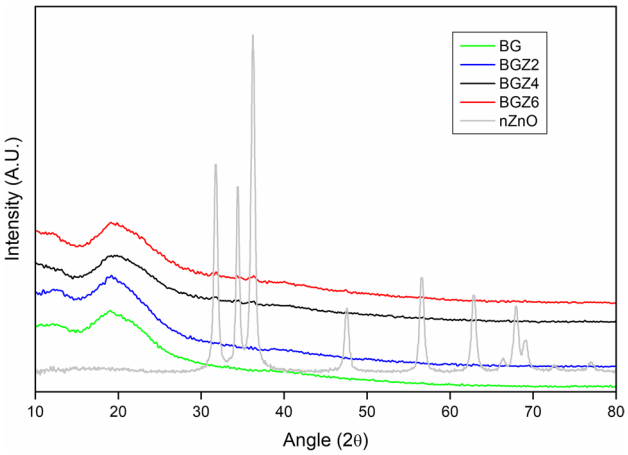

Fig. 3 X-ray diffractograms of BG and BGZ films

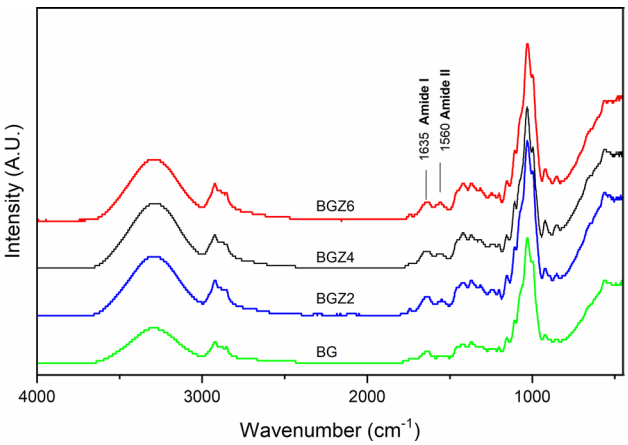

Fig. 4 ATR-FTIR spectra of BG and BGZ films

heat, stabilize the carbonaceous structure, and limit the diffusion of decomposition species [38].

The right side of Fig. 5 reports the DSC curves of the films. T_g of pure β-glucan films is around 90°, whereas it increases up to approximately 80 °C for the nanocomposite films. These values for the BG films are in agreement with literature data [39]. For BGZ films, a plasticizing effect of ZnO on the films was suggested in the previous study [26] as the cause of the decrease of the glass transition temperature. Here, the nZnO with a smaller size might have acted in the same capacity, promoting molecular mobility.

The optical properties of the films were characterized by UV–visible spectroscopy, and spectra are presented in Figure S2. The transmittance of the films is low, and the addition of nZnO further increases opacity both in the UV and in the visible range. This is widely reported for ZnO-containing composites [40].

3.2 Swelling Tests

Swelling ratios of BG and BGZ films are show in Fig. 6. The average SR of the samples is 80%. This value is comparable to the swelling ratios reported in the literature for crosslinked β-glucan hydrogels [41] and PVA/β-glucan hydrogels [42], as well as to the water absorption capacity of commercial hydrogels [43, 44].

Interestingly, neither nZnO content nor pH showed effects on the SR. The swelling of beta-glucan hydrogels is constrained by a multitude of intermolecular hydrogen bonds [41]. The lack of pH effect of SR suggests that the hydroxyl groups of the β-glucan macromolecules do not exhibit a strong tendency towards dissociation even at high pH values, or that the dissociation of hydroxyl moieties at high pH, if any, may not be sufficient to generate enough negative charges to cause electrostatic repulsion among molecules and to ultimately induce the expansion and swelling of the biopolymeric matrix.

This appears in contrast with the findings of Muthuramalingam and co-workers [42], who reported a four-fold increase in swelling ratio of PVA/β-glucan hydrogels at pH 9. However, this effect could be attributed to the prevalent content of PVA, which has been shown to exhibit enhanced swelling in alkaline environments [45].

Overall, this can be a positive aspect, as the insensitivity of BGZ films to pH and nZnO content allows their application in the presence of physiological fluids with very

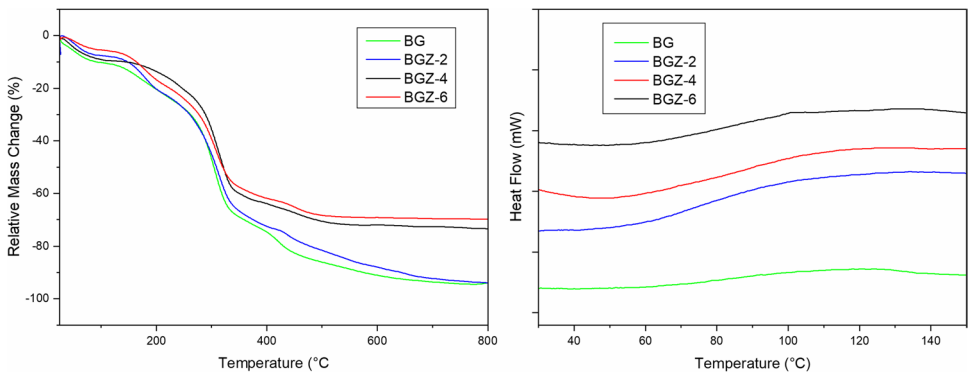

Fig. 5 TGA (left) and DSC (right) curves of BG and BGZ films

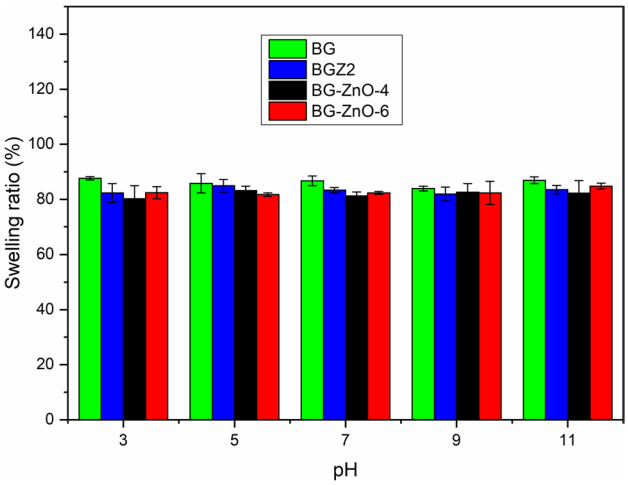

Fig. 6 Swelling ratio of BG and BGZ films in distilled water at different pH values

different acidity, such as sweat (around 4.5) and wound exudate (typically between 7.5 and 9). Moreover, nZnO content can be tuned to optimize other key properties without affecting the swelling ratio.

3.3 Antimicrobial Activity of nZnO

A preliminary evaluation of the antimicrobial activity of nZnO, which represents the antimicrobial agent purposely embedded in the beta-glucan matrix, has been carried out for the sake of completeness. Aqueous nZnO suspensions were tested having the following nanoparticles content: 30, 60, 120, 240, 480, 960, 1920, 3750, 7500, 15,000, 17,500, and 20,000 µg/mL.

The MIC and MBC values of nZnO against the tested bacteria are reported in Table 1. The MIC value found for *E. coli* was four-fold higher than that for *S. epidermidis*; moreover, the MBC related to the gram-negative bacterium was more than 7 times higher than that of the gram-positive one. These results show that nanostructured zinc oxide is more effective against *S. epidermidis* than against *E. coli*. They are in agreement with the literature [46] and can be attributed to the presence of the outer membrane in gram-negative bacteria that reduces the antibacterial action of ZnO.

MIC values of 64 and 300 µg/mL for ZnO nanorods were found by Jain and co-workers [47] against *S. aureus* (ATCC 2592) and *E. coli* (ATCC 25,922), respectively, using a spread plate method in which the nanorods were dispersed in the agar medium prior to the addition of the bacterial inoculum. The same study also showed how the presence of nano-zinc oxide in liquid cultures induces a concentration-dependent delay in the onset of the log phase of bacterial growth.

Table 1 Minimum inhibitory and minimum bactericidal concentrations of nZnO against *S. epidermidis* and *E. coli*

	MIC [µg/mL]	MBC [µg/mL]
S. epidermidis	120	480
E. coli	480	3750

Premanathan et al. [48] tested 30-nm acicular ZnO nanoparticles using the micro-broth dilution method against gram-negative *E. coli* (MTCC 739), gram-negative *P. aeruginosa* (MTCC 1688), and gram-positive *S. aureus* (MTCC 96), finding MICs of 500 µg/mL, 500 µg/mL, and 125 µg/mL, respectively.

3.4 Antimicrobial Activity of Composite Films

The antimicrobial activity of the BG, BGZ-2, BGZ-4, and BGZ-6 films has been tested against both *S. epidermids* and *E. coli*, and the results are shown in Figs. 7 and 8. β-glucans have been frequently tested in the literature against different microbial strains. Song and Chamidah reported antimicrobial activity of β-glucans from naked barley bran and *Sargassum crassifolium*, respectively [49, 50]. Khan and co-workers demonstrated the antimicrobial activity of β-glucans derived from *S. cerevisiae* too [51]. β-glucans are found to penetrate bacterial cells interfering with their metabolism and inducing cellular lysis [41]. However, β-glucans antimicrobial effects vary quite widely depending on their purity, origin, molecular weight, structural conformation, and chemical modification, as well as on the microbial strains [49]–[51]. Moreover, the above-mentioned studies tested β-glucans in liquid suspensions, which might be substantially different from β-glucans in the form of solid films. In fact, as the polysaccharide molecules are immobilized as part of the film structure, it can be envisaged that their diffusion and consequent penetration of the bacterial cells would be prevented. As an additional consequence, a large fraction of potentially bioactive functional groups would be masked or engaged in intermolecular interactions.β-glucan films did not show intrinsic antimicrobial activity. On the contrary, all BGZ films show an antibacterial activity against *S. epidermidis* (Fig. 7), which appears to be nZnO concentration dependent (Fig. 8), whereas no activity against *E. coli* was observed. The higher activity of BGZ films on *S. epidermidis* than on *E. coli* is in agreement with the results of antimicrobial tests on nZnO as such, previously discussed. Moreover, the higher activity of the nanocomposite films on the gram-positive is in accordance with the results of Razzaq et al. on BG-ZnO composite films [26]. A comparison with other literature studies can also be made. Azari et al. [14] reported the preparation of gelatin/β-glucan/ZnO composite films

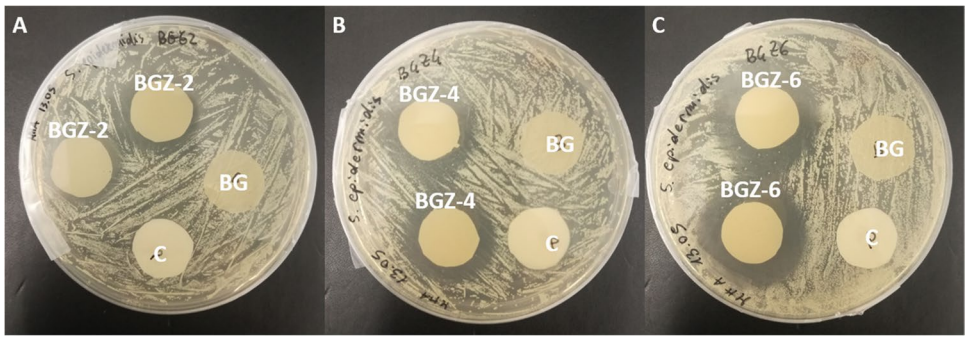

Fig. 7 Disk diffusion test of **A** BGZ-2, **B** BGZ-4, and **C** BGZ-6 film samples against *S.epidermidis.* C indicates the filter paper control disc

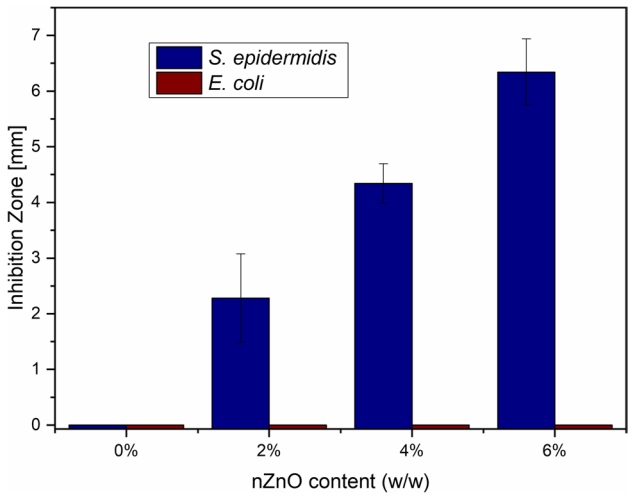

Fig. 8 Inhibition zone values of BG and BGZ films against *S.epidermidis* and *E.coli*

which shown antibacterial properties against *P. aeruginosa*, *S. typhimorium*, *S. aureus*, and *E. coli*. The researchers used the disk diffusion test and obtained inhibition zones of 14.2 ± 1.32, 13.2 ± 1.72, 17.0 ± 2.10, and 15.0 ± 1.52 mm against the abovementioned microorganisms, respectively, for a composite containing 5% w/w nano-ZnO. Also in this case, antimicrobial effects were more marked on the gram-positive specie and could be correlated to the concentration of ZnO nanoparticles, whereas increases in the β-glucan content did not produce any significative improvement in antibacterial effects. Arfat [38] tested 10-mm fish protein isolate/fish skin gelatin disks with 3% nano-ZnO against *L. monocytogenes*, reporting zones of inhibition of about 22 mm. It shall be noted that these studies did not carry the antibacterial tests against the same microbial strains. Also note that these inhibition zone values are expressed as the total diameter of the inhibited-growth zone and not as the length between the disk perimeter and the end of the inhibition zone, as in our case. This being considered, the values reported are in general comparable and testify a good effectiveness of the materials described in this work. A direct comparison can instead be made with our previous work on whey protein isolate-nZnO composite films [30]. Despite having a lower swelling ratio and transparency, BGZ composites were able to achieve a higher inhibition zone with a smaller quantity of embedded nZnO, showing how a β-glucan matrix can in fact be very well suited for an antibacterial wound dressing.

4 Conclusions

Antibacterial bionanocomposite films have been developed for the first time by combining β-glucans from *S. cerevisiae* and nanostructured zinc oxide, using glycerol as a plasticizer. The adopted procedure led to good solubilization of the β-glucans in water and to the subsequent formation of a flexible polysaccharide-based material, thus eliminating the need for crosslinking substances and toxic solvents. ZnO nanoparticles were dispersed inside the fims, and they did not affect the key functional properties such as the swelling ratio that is comparable with existing wound dressing solutions, both commercial and reported in the literature. The antibacterial activity was particularly evident against the gram-positive *S. epidermidis*, and it was directly dependent to nZnO concentration. On the contrary, the effect against the gram-negative *E. coli* was negligible. Considering the abundance and the beneficial properties of β-glucans, this study lays solid grounds for further in-vitro and in-vivo investigation of cytotoxicity and wound healing potential of these materials, towards the development of targeted solutions for skin tissue engineering and regeneration.

Supplementary Information The online version contains supplementary material available at https://doi.org/10.1007/s12668-023-01079-0.

Author Contribution PP wrote the main manuscript text and prepared the figures with the help of GP. PP and GP conducted the experimental activities. CM contributed to writing Sects. 2.7, 2.8, 3.3, and 3.4 and helped in designing, organizing, and carrying out the related experimental activities. SR contributed to writing Sects. 2.2, 2.5, and 3.1 and interpreting the related results. BO and FB conceptualized, coordinated, and supervised the activities. All authors reviewed the manuscript.

Funding Open access funding provided by Politecnico di Torino within the CRUI-CARE Agreement.

Data Availability N/A.

Declarations

Ethics Approval and Consent to Participate N/A.

Consent for Publication N/A.

Competing Interests The authors declare no competing interests.

References

1. Sen, C. K., et al. (2009). Human skin wounds: A major and snowballing threat to public health and the economy: PERSPECTIVE ARTICLE. *Wound Repair and Regeneration, 17*(6), 763–771. https://doi.org/10.1111/j.1524-475X.2009.00543.x
2. C. K. Sen, "Human wounds and its burden: An updated compendium of estimates," *Advances in Wound Care*, vol. 8, no. 2. Mary Ann Liebert Inc., pp. 39–48, Feb. 01, 2019. https://doi.org/10.1089/wound.2019.0946.
3. Yao, G., et al. (2022). A programmable and skin temperature–activated electromechanical synergistic dressing for effective wound healing. *Science Advances, 8*(4), 8379. https://doi.org/10.1126/SCIADV.ABL8379/SUPPL_FILE/SCIADV.ABL8379_MOVIES_S1_TO_S3.ZIP
4. Russo, S., Landi, S., & Courric, S. (2022). Cost-effectiveness analysis for the treatment of diabetic foot ulcer in France: Platelet-rich plasma vs standard of care. *ClinicoEconomics and Outcomes Research, 14*, 1–10. https://doi.org/10.2147/CEOR.S327191
5. Mirhaj, M., Labbaf, S., Tavakoli, M., & Seifalian, A. (2022). An overview on the recent advances in the treatment of infected wounds: Antibacterial wound dressings. *Macromolecular Bioscience, 22*(7), 2200014. https://doi.org/10.1002/MABI.202200014
6. "Advanced wound dressing market size report, 2021–2028." https://www.grandviewresearch.com/industry-analysis/advanced-wound-care-dressing-market (accessed Jan. 24, 2021).
7. R. Esmaeely Neisiany, M. S. Enayati, P. Sajkiewicz, Z. Pahlevanneshan, and S. Ramakrishna, "Insight into the current directions in functionalized nanocomposite hydrogels," *Front Mater*, vol. 7, Feb. 2020. https://doi.org/10.3389/fmats.2020.00025.
8. E. M. Tottoli, R. Dorati, I. Genta, E. Chiesa, S. Pisani, and B. Conti, "Skin wound healing process and new emerging technologies for skin wound care and regeneration," *Pharmaceutics*, vol. 12, no. 8. MDPI AG, pp. 1–30, Aug. 01, 2020. https://doi.org/10.3390/pharmaceutics12080735.
9. Ma, J., & Underhill, D. M. (2013). β-glucan signaling connects phagocytosis to autophagy. *Glycobiology, 23*(9), 1047–1051. https://doi.org/10.1093/GLYCOB/CWT046
10. van den Berg, L. M., Zijlstra-Willems, E. M., Richters, C. D., Ulrich, M. M. W., & Geijtenbeek, T. B. H. (2014). Dectin-1 activation induces proliferation and migration of human keratinocytes enhancing wound re-epithelialization. *Cellular Immunology, 289*(1–2), 49–54. https://doi.org/10.1016/J.CELLIMM.2014.03.007
11. Du, B., Bian, Z., & Xu, B. (2014). Skin health promotion effects of natural beta-glucan derived from cereals and microorganisms: A review. *Phytotherapy Research, 28*(2), 159–166. https://doi.org/10.1002/PTR.4963
12. Grip, J., et al. (2018). Beta-glucan-loaded nanofiber dressing improves wound healing in diabetic mice. *European Journal of Pharmaceutical Sciences, 121*, 269–280. https://doi.org/10.1016/J.EJPS.2018.05.031
13. Grip, J., Engstad, R. E., Skjæveland, I., Škalko-Basnet, N., & Holsæter, A. M. (2017). Sprayable carbopol hydrogel with soluble beta-1,3/1,6-glucan as an active ingredient for wound healing – development and in-vivo evaluation. *European Journal of Pharmaceutical Sciences, 107*, 24–31. https://doi.org/10.1016/J.EJPS.2017.06.029
14. Sherafatkhah Azari, S., Alizadeh, A., Roufegarinejad, L., Asefi, N., & Hamishehkar, H. (2021). "Preparation and characterization of gelatin/β-glucan nanocomposite film incorporated with ZnO nanoparticles as an active food packaging system." *J Polym Environ, 29*(4), 1143–1152. https://doi.org/10.1007/s10924-020-01950-1
15. Huang, M. H., & Yang, M. C. (2008). Evaluation of glucan/poly(vinyl alcohol) blend wound dressing using rat models. *International Journal of Pharmaceutics, 346*(1–2), 38–46. https://doi.org/10.1016/j.ijpharm.2007.06.021
16. Sagnelli, D., et al. (2017). All-natural bio-plastics using starch-betaglucan composites. *Carbohydrate Polymers, 172*, 237–245. https://doi.org/10.1016/j.carbpol.2017.05.043
17. Chang, J., et al. (2019). Preparation, properties, and structural characterization of β-glucan/pullulan blend films. *International Journal of Biological Macromolecules, 140*, 1269–1276. https://doi.org/10.1016/j.ijbiomac.2019.08.208
18. Hunt, S. D. (2018). "A clinical observation evaluation of bioactive soluble beta-glucan gel compared with standard care." *J Wound Care, 27*(9), 620–630. https://doi.org/10.12968/jowc.2018.27.9.620
19. Elg, F., Posnett, J., & Hunt, S. (2019). "Cost-effectiveness of soluble beta-glucan gel in hard-to-heal wounds: An evaluation." *J Wound Care, 28*(7), 454–460. https://doi.org/10.12968/jowc.2019.28.7.454
20. J. Hurlow and P. G. Bowler, "Acute and chronic wound infections: microbiological, immunological, clinical and therapeutic distinctions," *J Wound Care*, vol. 31, no. 5, pp. 436–445, May 2022. https://doi.org/10.12968/JOWC.2022.31.5.436/ASSET/IMAGES/LARGE/JOWC.2022.31.5.436_F06.JPEG.
21. M. Alavi and A. Nokhodchi, "An overview on antimicrobial and wound healing properties of ZnO nanobiofilms, hydrogels, and bionanocomposites based on cellulose, chitosan, and alginate polymers," *Carbohydrate Polymers*, vol. 227. Elsevier Ltd, p. 115349, Jan. 01, 2020. https://doi.org/10.1016/j.carbpol.2019.115349.
22. Jiang, J., Pi, J., & Cai, J. (2018). The advancing of zinc oxide nanoparticles for biomedical applications. *Bioinorganic Chemistry and Applications*. https://doi.org/10.1155/2018/1062562
23. Kaushik, M., et al. (2019). Investigations on the antimicrobial activity and wound healing potential of ZnO nanoparticles. *Applied Surface Science, 479*, 1169–1177. https://doi.org/10.1016/J.APSUSC.2019.02.189
24. A. Kushwaha, L. Goswami, and B. S. Kim, "Nanomaterial-based therapy for wound healing," *Nanomaterials 2022, Vol.*

12, Page 618, vol. 12, no. 4, p. 618, Feb. 2022. https://doi.org/10.3390/NANO12040618.
25. M. M. Mihai, M. B. Dima, B. Dima, and A. M. Holban, "Nanomaterials for wound healing and infection control," *Materials 2019, Vol. 12, Page 2176*, vol. 12, no. 13, p. 2176, Jul. 2019. https://doi.org/10.3390/MA12132176.
26. H. A. A. Razzaq *et al.*, "Bioactive films based on barley β-glucans and ZnO for wound healing applications," *Carbohydr Polym*, vol. 272, p. 118442, Nov. 2021. https://doi.org/10.1016/J.CARBPOL.2021.118442.
27. Sirelkhatim, A., et al. (2015). Review on zinc oxide nanoparticles: Antibacterial activity and toxicity mechanism. *Nanomicro Lett, 7*(3), 219–242. https://doi.org/10.1007/s40820-015-0040-x
28. J. Majtan and M. Jesenak, "β-glucans: Multi-functional modulator of wound healing," *Molecules 2018, Vol. 23, Page 806*, vol. 23, no. 4, p. 806, Apr. 2018. https://doi.org/10.3390/MOLECULES23040806.
29. Q. Wang *et al.*, "β-glucans: Relationships between modification, conformation and functional activities," *Molecules 2017, Vol. 22, Page 257*, vol. 22, no. 2, p. 257, Feb. 2017. https://doi.org/10.3390/MOLECULES22020257.
30. P. Pino, S. Ronchetti, C. Mollea, M. Sangermano, B. Onida, and F. Bosco, "Whey proteins–zinc oxide bionanocomposite as antibacterial films," *Pharmaceutics 2021, Vol. 13, Page 1426*, vol. 13, no. 9, p. 1426, Sep. 2021. https://doi.org/10.3390/PHARMACEUTICS13091426.
31. "EUCAST reading guide for broth microdilution," 2022, Accessed: Apr. 21, 2022. www.eucast.org
32. "EUCAST: Disk diffusion methodology." https://www.eucast.org/ast_of_bacteria/disk_diffusion_methodology/ (accessed Nov. 25, 2020).
33. J. Winiarski, W. Tylus, K. Winiarska, I. Szczygieł, and B. Szczygieł, "XPS and FT-IR characterization of selected synthetic corrosion products of zinc expected in neutral environment containing chloride ions," *Journal of Spectroscopy*, vol. 2018, 2018. https://doi.org/10.1155/2018/2079278.
34. Banchero, M., et al. (2019). Supercritical solvent impregnation of different drugs in mesoporous nanostructured zno. *Pharmaceutics, 11*(7), 1–14. https://doi.org/10.3390/pharmaceutics11070340
35. G. Socratres, *Infrared and Raman characteristic group frequencies*, Third., vol. 5, no. 2. Wiley, 2001. https://doi.org/10.1016/0160-9327(81)90159-9.
36. Nováka, M., et al. (2012). Yeast β(1–3), (1–6)-d-glucan films: Preparation and characterization of some structural and physical properties. *Carbohydrate Polymers, 87*(4), 2496–2504. https://doi.org/10.1016/j.carbpol.2011.11.031
37. Kacuráková, M., Capek, P., Sasinková, V., Wellner, N., & Ebringerová, A. (2000). FT-IR study of plant cell wall model compounds: Pectic polysaccharides and hemicelluloses. *Carbohydrate Polymers, 43*(2), 195–203. https://doi.org/10.1016/S0144-8617(00)00151-X
38. Arfat, Y. A., Benjakul, S., Prodpran, T., Sumpavapol, P., & Songtipya, P. (2014). Properties and antimicrobial activity of fish protein isolate/fish skin gelatin film containing basil leaf essential oil and zinc oxide nanoparticles. *Food Hydrocoll, 41*, 265–273. https://doi.org/10.1016/j.foodhyd.2014.04.023
39. Razzaq, H. A. A., et al. (2016). Barley β-glucan-protein based bioplastic film with enhanced physicochemical properties for packaging. *Food Hydrocoll, 58*, 276–283. https://doi.org/10.1016/j.foodhyd.2016.03.003
40. Vaezi, K., Asadpour, G., & Sharifi, H. (2019). Effect of ZnO nanoparticles on the mechanical, barrier and optical properties of thermoplastic cationic starch/montmorillonite biodegradable films. *International Journal of Biological Macromolecules, 124*, 519–529. https://doi.org/10.1016/j.ijbiomac.2018.11.142
41. Y. Matsumoto, Y. Enomoto, S. Kimura, and T. Iwata, "Highly deformable and recoverable cross-linked hydrogels of 1,3-α-D and 1,3-β-D-glucans," *Carbohydr Polym*, vol. 251, no. July 2020, p. 116794, 2021. https://doi.org/10.1016/j.carbpol.2020.116794.
42. Muthuramalingam, K., Choi, S. I., Hyun, C., Kim, Y. M., & Cho, M. (2019). β-glucan-based wet dressing for cutaneous wound healing. *Adv Wound Care (New Rochelle), 8*(4), 125–135. https://doi.org/10.1089/WOUND.2018.0843/ASSET/IMAGES/LARGE/FIGURE5.JPEG
43. "Neoheal - KIKGEL." https://kikgel.com.pl/en/products/neoheal/#advantages-of-neoheal--hydrogel-dressing (accessed Nov. 10, 2021).
44. Lee, O. J., et al. (2016). Fabrication and characterization of hydrocolloid dressing with silk fibroin nanoparticles for wound healing. *Tissue Eng Regen Med, 13*(3), 218–226. https://doi.org/10.1007/s13770-016-9058-5
45. Minhas, M. U., Ahmad, M., Ali, L., & Sohail, M. (2013). Synthesis of chemically cross-linked polyvinyl alcohol-co-poly (methacrylic acid) hydrogels by copolymerization; A potential graft-polymeric carrier for oral delivery of 5-fluorouracil. *DARU, Journal of Pharmaceutical Sciences, 21*(1), 1–9. https://doi.org/10.1186/2008-2231-21-44/TABLES/3
46. R. Kumar, A. Umar, G. Kumar, and H. S. Nalwa, "Antimicrobial properties of ZnO nanomaterials: A review," *Ceramics International*, vol. 43, no. 5. Elsevier Ltd, pp. 3940–3961, Apr. 01, 2017. https://doi.org/10.1016/j.ceramint.2016.12.062.
47. Jain, A., Bhargava, R., & Poddar, P. (2013). Probing interaction of gram-positive and gram-negative bacterial cells with ZnO nanorods. *Materials Science and Engineering C, 33*(3), 1247–1253. https://doi.org/10.1016/j.msec.2012.12.019
48. Premanathan, M., Karthikeyan, K., Jeyasubramanian, K., & Manivannan, G. (2011). Selective toxicity of ZnO nanoparticles toward gram-positive bacteria and cancer cells by apoptosis through lipid peroxidation. *Nanomedicine, 7*(2), 184–192. https://doi.org/10.1016/J.NANO.2010.10.001
49. J. Song, H. Chen, Y. Wei, and J. Liu, "Synthesis of carboxymethylated β-glucan from naked barley bran and its antibacterial activity and mechanism against Staphylococcus aureus," *Carbohydr Polym*, vol. 242, p. 116418, Aug. 2020. https://doi.org/10.1016/J.CARBPOL.2020.116418.
50. A. Chamidah, Hardoko, and A. A. Prihanto, "Antibacterial activities of β-glucan (laminaran) against gram-negative and gram-positive bacteria," *AIP Conf Proc*, vol. 1844, no. May, 2017. https://doi.org/10.1063/1.4983422.
51. Khan, A. A., et al. (2016). Structural, thermal, functional, antioxidant & antimicrobial properties of β-d-glucan extracted from baker's yeast (Saccharomyces cereviseae)—effect of γ-irradiation. *Carbohydrate Polymers, 140*, 442–450. https://doi.org/10.1016/J.CARBPOL.2016.01.003